European Journal of Medicinal Chemistry 58 (2012) 272–280

Contents lists available at SciVerse ScienceDirect

European Journal of Medicinal Chemistry

journal homepage: http://www.elsevier.com/locate/ejmech

Original article

Synthesis, *in silico*, *in vitro*, and *in vivo* investigation of 5-[^{11}C]methoxy-substituted sunitinib, a tyrosine kinase inhibitor of VEGFR-2

Julio Caballero [a], Camila Muñoz [a], Jans H. Alzate-Morales [a], Susana Cunha [b], Lurdes Gano [b], Ralf Bergmann [c], Joerg Steinbach [c], Torsten Kniess [c,*]

[a] Centro de Bioinformática y Simulación Molecular, Universidad de Talca, 2 Norte 685, Casilla 721, Talca, Chile
[b] Unidade de Ciências Químicas e Radiofarmacêuticas, IST/ITN, Instituto Superior Técnico, Universidade Técnica de Lisboa, Estrada Nacional 10, 2686-953 Sacavém, Portugal
[c] Institute of Radiopharmacy, Helmholtz-Zentrum Dresden-Rossendorf e.V., POB 510119, D-01314 Dresden, Germany

ARTICLE INFO

Article history:
Received 12 March 2012
Received in revised form
5 October 2012
Accepted 11 October 2012
Available online 23 October 2012

Keywords:
Sunitinib®
VEGFR
Docking
Molecular dynamics
MM-GBSA
Carbon-11
Radiolabeling

ABSTRACT

Sunitinib® (SU11248) is a highly potent tyrosine kinase inhibitor targeting vascular endothelial growth factor receptor (VEGFR). Radiolabeled inhibitors of receptor tyrosine kinases (RTKs) might be useful tools for monitoring RTKs levels in tumor tissue giving valuable information for anti-angiogenic therapy. Herein we report the synthesis of 5-methoxy-sunitinib **5** and its ^{11}C-radiolabeled analog [^{11}C]-**5**. The non-radioactive reference compound **5** was prepared by Knoevenagel condensation of 5-methoxy-2-oxindole with the corresponding substituted 5-formyl-1*H*-pyrrole. A binding constant (K_d) of 20 nM for **5** was determined by competition binding assay against VEGFR-2. In addition, the binding mode of sunitinib® and its 5-methoxy substituted derivative was studied by flexible docking simulations. These studies revealed that the substitution of the fluorine at position 5 of the oxindole scaffold by a methoxy group did not affect the inhibitor orientation, but affected the electrostatic and van der Waals interactions of the ligand with residues near the DFG motif of VEGFR-2. 5-[^{11}C]methoxy-sunitinib ([^{11}C]-**5**) was synthesized by reaction of the desmethyl precursor with [^{11}C]CH_3I in the presence of DMF and NaOH in 17 ± 3% decay-corrected radiochemical yield at a specific activity of 162–205 GBq/μmol (EOS). *In vivo* stability studies of [^{11}C]-**5** in rat blood showed that more than 70% of the injected compound was in blood stream, 60 min after administration.

1. Introduction

Angiogenesis is a well regulated physiological process involving the growth of new blood vessels from pre-existing vascular and capillary networks in vital mechanisms like wound healing. However it is also a transitional step in the development of tumors because cancer cells are generally limited to a diameter of 2–3 mm without additional blood supply, so tumors often promote local angiogenesis to support their growth and nutrition. A number of pro- and anti-angiogenic factors shift the micro milieu of the tumor cell in the favor of vessel development and consequently markers of increased angiogenesis have been recognized as effective targets for therapeutics as well as novel means of imaging of cancer [1,2].

The vascular endothelial growth factor (VEGF) is a key regulator of neovascularization and an elevated level of VEGF is known to correlate with increased metastatic invasion [3]. Among the VEGF receptor kinases types VEGFR-2 is believed to be the key transducer for angiogenic and mitogenic properties [4]. Anti-angiogenic therapies focus on targeted inhibition of overexpressed growth factors with the aim of suppressing tumor growth. This inhibition has been attempted by either blocking the extracellular ligand binding domain of the receptor with antibodies, affibodies or peptides or by inhibition of the intracellular tyrosine kinase at the adenosine triphosphate (ATP) binding site with small molecule inhibitors [5]. Such targeted tumor therapies are accompanied with a more sensitive need for dose optimization and monitoring of the therapeutic response. Direct non-invasive molecular imaging of tumor vascularization and angiogenic processes *in vivo* would facilitate the selection of patients and help to evaluate the efficacy of anti-angiogenic therapies, due to the fact that anti-angiogenic agents are generally cytostatic and do necessarily cause large reductions in tumor volume on a short time scale even when they are effective [6]. Radionuclide-based imaging technologies, like positron emission tomography (PET) and single photon emission computed

* Corresponding author.
E-mail address: t.kniess@hzdr.de (T. Kniess).

0223-5234/$ – see front matter © 2012 Elsevier Masson SAS. All rights reserved.
http://dx.doi.org/10.1016/j.ejmech.2012.10.020

tomography (SPECT) are progressively affecting the clinical diagnosis and treatment of cancer. These techniques are based on the concept that diagnostic radiotracers will accumulate in specific tissues altered in a diseased situation due to interaction at molecular level [7]. Direct non-invasive molecular imaging and reliable quantitative method to determine *in vivo* the levels of VEGFR expression would help to evaluate the efficacy of anti-angiogenic therapies and facilitate the selection of patients for a customized VEGFR-targeted cancer treatment. Consequently radiolabeled peptide markers (RGD), radiolabeled antibodies (bevacizumab) and radiolabeled small molecule receptor tyrosine kinase inhibitors have been developed as radioactive probes for imaging anti-angiogenic therapies; for detailed information on this field a number of excellent reviews may be considered [5,7–9].

Radiotracers targeting VEGFR tyrosine kinase would provide useful information about location and density of these receptors by molecular imaging and would assist in the therapy of VEGFR positive tumors. Consequently known VEGFR inhibitors like vandetanib®, Ki8751, sorafenib® and brivanib® as well as diaryl-substituted maleimide derivatives have been selected for radiolabeling preferably with the positron emitters carbon-11 and fluorine-18 [10–16]. The multi-targeted kinase inhibitor sunitinib® inhibits VEGFR-2 in the low nanomolar range and was approved as anti-angiogenic drug for treatment of renal cell carcinoma and gastrointestinal stromal drugs in 2006 (Fig. 1). The radiosynthesis of the fluorine-18 labeled sunitinib® has been described; however no radiopharmacological data were published up to now [17]. Our laboratory has contributed to this scientific area by designing and synthesizing an ^{18}F-labeled analog of SU5202, a VEGFR inhibitor in the micromolar range [18,19] and recently with a ^{125}I-labeled sunitinib derivative [20].

Owed to the chemical structure of sunitinib® that gives less possibility for further substitution with [^{18}F]fluoride we aimed in our ongoing studies to design a methoxy-substituted derivative near to the sunitinib® lead structure and to develop a carbon-11 labeled radiotracer for imaging VEGFR-2.

The present paper describes the synthesis of 5-methoxy-substituted sunitinib® (Fig. 1), its ability to inhibit VEGFR-2 assessment both *in vitro* and *in vivo* in cell models as well as the radiosynthesis of the ^{11}C-radiolabeled analog and its preliminary *in vivo* stability evaluation. Studies on the binding modes of both ligands inside the active site of VEGFR-2 were also carried out by docking simulations and are reported herein.

2. Chemistry

The synthetic strategy for preparation of the non-radioactive reference compound, 5-methoxy-substituted sunitinib **5** as well as of the corresponding desmethyl precursor **4** for ^{11}C-radiolabeling is outlined at Scheme 1. The key starting compound 5-hydroxy-oxindole **1** is not commercially available and its synthesis was hitherto described in the literature via a laborious 5-step synthesis starting from *p*-anisidine [21]. To circumvent this drawback hypervalent iodine reagents have been used for the oxidation of phenols and anilines and recently the convenient synthesis of 5-hydroxy-oxindole **1** in a single step from oxindole with phenyliodine(III)-bis(trifluoroacetate) PIFA was reported [22]. Following this procedure the desired 5-hydroxy-oxindole **1** was obtained in 70% chemical yield in high purity after purification by column chromatography. Selective O-methylation of **1** was achieved by using dimethyl sulfate in the presence of potassium hydroxide as described by Laksmaiah et al. [23] to afford 5-methoxy-oxindole **2**. However during this reaction several by-products were formed affording **2** in a chemical yield that did not exceed 35%, after column chromatography purification. Finally, each oxindole derivative **1** and **2** reacted with *N*-[2-(diethylamino) ethyl]-2,4-dimethyl-5-formyl-1*H*-pyrrole-3-carboxamide **3** [24] via Knoevenagel condensation, in the presence of ethanol and piperidine. In this way the 5-hydroxy-substituted sunitinib **4** and its 5-methoxy substituted derivative **5** were obtained as pure compounds and no further purification was required.

3. Docking simulations

Rigid docking simulations were performed by using Glide [25]. Characteristics of Glide docking method have been described in previous reports [26]. The previously reported model of VEGFR-2 derived from the X-ray crystal structure (accession code in Protein Data Bank (PDB): 3ewh) with the activation loop modeled was used as the protein receptor in docking experiments [19]. The structures of sunitinib® and compound **5** were sketched by using Maestro software [27]. The docking poses for each ligand were analyzed by examining their relative total energy score. The more energetically favorable conformation was selected as the best pose.

Molecular dynamics (MD) simulations of sunitinib® and compound **5** inside VEGFR-2 active site were studied using the OPLS-AA force field in explicit solvent with the SPC water model (OPLS-AA/SPC) [28], within the Desmond program [29] for MD simulations. The initial coordinates for the MD calculations were taken from the docking experiments. The SPC water molecules were then added (the dimensions of each orthorhombic water box were 84 Å × 79 Å × 65 Å approximately, which ensured the whole surfaces of the complexes to be covered by solvent model) and the systems were neutralized by adding chloride counter ions to balance the net charges of the systems. Before equilibration and

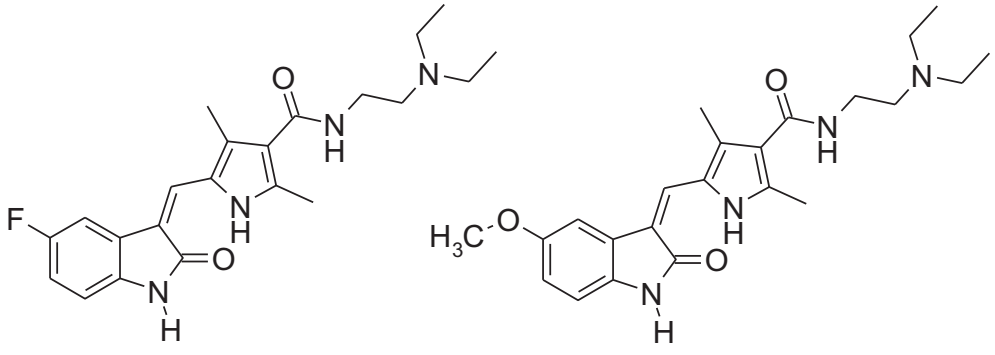

Fig. 1. Structures of sunitinib® and 5-methoxy-sunitinib.

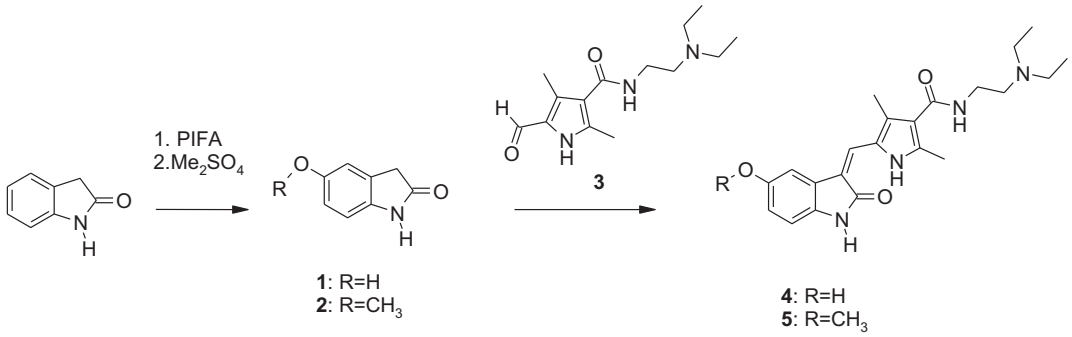

Scheme 1. Synthesis of labeling precursor **4** and reference compound **5**.

long production MD simulations, the systems were minimized and pre-equilibrated using the default relaxation routine implemented in Desmond. For this, the program ran six steps composed of minimizations and short (12 and 24 ps) MD simulations to relax the model system before performing the final long simulations. After that, a first 5 ns long equilibration MD simulation was performed on each complex system. To check whether the equilibrated MD trajectory was stable, RMSD values of side-chain heavy atoms with respect to the initial coordinates were tested. Then, a 20 ns long production MD simulation was performed. The OPLS-2005 [28] force field was used, along with module MacroModel [30] to provide and check the necessary force field parameters for the ligands. When MacroModel performs an energy calculation, the program checks the quality of each parameter in use. All, bond, angle, torsional and improper checked parameters were listed as high and medium quality force field parameters for all ligands studied. During MD simulations, the equations of motion were integrated with a 2-fs time step in the NVT ensemble. The SHAKE algorithm was applied to all hydrogen atoms; the VDW cutoff was set to 9 Å. The temperature was maintained at 300 K, employing the Nosé–Hoover thermostat method with a relaxation time of 1 ps. Long-range electrostatic forces were taken into account by means of the particle-mesh Ewald (PME) approach. Data were collected every 1 ps during the MD runs. Visualization of protein–ligand complexes and MD trajectory analysis were carried out with the VMD software package [31].

4. Results and discussion

4.1. Inhibition of tyrosine kinase activity

Due to the lack of information concerning the inhibitory properties of the new synthesized 5-methoxy-substituted sunitinib **5** the compound was submitted to a comprehensive test system for screening compounds against large number of human kinases, KINOME*scan*™. This system is based on a competition binding assay that quantitatively measures the ability of a compound to compete with an immobilized, active-site directed ligand. The assay is performed by combining three components: DNA-tagged kinase; immobilized ligand and the test compound. The ability of the test compound to compete with the immobilized ligand is measured via quantitative PCR of the DNA tag [32].

For testing 5-methoxy-substituted sunitinib **5** against VEGFR-2 an 11-point 3-fold serial dilution of **5** was prepared in 100% DMSO at 100 × final test concentration and subsequently diluted to 1× in the assay (final DMSO concentration = 2.5%). The binding constant (K_d) was calculated with a standard dose–response curve using the Hill equation, curves were fitted using a non-linear least square fit with the Levenberg–Marquardt algorithm. Fig. 2 displays the curve image for 5-methoxy-substituted sunitinib **5**, the amount of kinase measured by qPCR (*y*-axis) is plotted against the concentration of **5** in nM in log 10 scale (*x*-axis). In a duplicated experimental determination a K_d value of 20 nM for 5-methoxy-substituted sunitinib **5** for the inhibition of VEGFR-2 was found. This K_d value is adequately low to justify classification of **5** as an inhibitor of VEGFR-2, as for the lead compound Sunitinib a K_i value of 9 nM is published [33].

4.2. Inhibition of cell proliferation

The potency of **5** to inhibit cell proliferation was assessed by the colorimetric MTT assay in two VEGFR expressing cell lines, primary endothelial HAEC and cancer HT29. This assay measures the amount of tetrazolium dye (MTT) reduced by a mitochondrial dehydrogenase located in the inner mitochondrial membrane of viable cells that is involved in the oxidative phosphorylation. Thus, cell viability is proportional to the reduction of MTT. The proliferation inhibitory activity of the compound was evaluated by determination of the IC_{50}, the concentration needed to inhibit cell proliferation by 50%, determined through dose–response curves achieved from percentage of cell proliferation plotted against the corresponding compound concentration. IC_{50} values are presented in Table 1, in comparison with the values found for sunitinib® in the same experimental conditions.

Analysis of these results shows the compounds potency to inhibit the tyrosine kinase activity as well as its ability to cross the cell membrane. As expected, the results indicated that 5-methoxy-sunitinib is able to cross the cell membrane and to inhibit the cell propagation. Nevertheless the IC_{50} values analysis in comparison with the parent compound shows that its potency as inhibitor is lower than that of sunitinib®. On the other hand the ability to inhibit the cell proliferation also depends on the cell line. In general

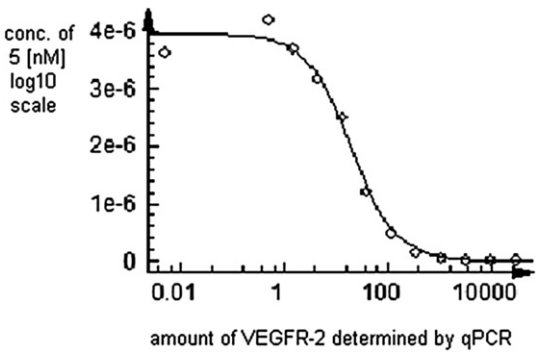

Fig. 2. Curve of inhibition of 5-methoxy-sunitinib **5** against VEGFR-2.

Table 1
Inhibition of cell proliferation.

Compound	Inhibition of cell proliferation IC_{50} (μM)	
	HAEC	HT29
5	54.8 ± 0.06	7.88 ± 0.06
Sunitinib	0.10 ± 0.07	0.33 ± 0.02

these findings, in both cell lines, are in agreement with the VEGFR-2 competition binding studies.

4.3. Docking results

Our docking methodology consists of two steps: first, the complexes were obtained by rigid docking, and then the movement of the complexes was studied by MD simulations. The orientations obtained by docking experiments were compared with the X-ray crystallographic structure of the complex between KIT and sunitinib® (accession code in PDB: 3g0e) [34]. Active sites of KIT and VEGFR-2 are very similar; in this sense, we expected that oxindole scaffold should be oriented inside VEGFR-2's active site in a similar manner with respect to the orientation in KIT. Therefore, the orientations obtained by docking experiments carried out inside VEGFR-2's active site were compared with the X-ray crystallographic structure of complex between KIT and the oxindole scaffold of sunitinib®. The values of the root-mean square deviations (RMSDs) for the docked structures of sunitinib® and its 5-methoxy-derivative **5** with respect to the X-ray crystal inhibitor structure (considering the 2,4-dimethyl-5-[(*Z*)-(2-oxo-1,2-dihydro-3*H*-indol-3-ylidene)methyl]-1*H*-pyrrole-3-carboxamide moiety in KIT) were 0.288 and 0.879 Å, respectively. According to this, we can conclude that the docked structures showed the same orientation for inhibitors in VEGFR-2 with respect to the known orientation of the oxindole scaffold in KIT. Furthermore, the change of the fluoro- by the methoxy-substituent at 5-position of the oxindole scaffold does not affect the orientation of the inhibitor. Thus, compound **5** keeps the interactions of a potent VEGFR-2 inhibitor.

Both inhibitors (sunitinib® and 5-methoxy-sunitinib **5**) adopted the same binding mode; this is not surprising because both compounds contain the same scaffold and similar substituents. In both compounds: i) the oxindole scaffold is surrounded by residues Phe1047, Val848, Ala866, Lys868, Val899, Glu917, Phe918, Cys919, and Leu840, and it forms hydrogen bond (HB) interactions between the NH of the oxindole and the backbone carbonyl group of Glu917, and between the carbonyl of the oxindole and the backbone NH of Cys919, ii) 3,5-dimethyl-1*H*-pyrrol-2-yl group is at the entrance of the pocket and is surrounded by residues Leu840, Phe1047, Phe918, Gly922, and Asn923, iii) the group {[2-(diethylamino)ethyl]amino} carbonyl is exposed to the solvent media, and iv) the groups at position 5 of oxindole scaffold (F or OCH_3), which are responsible of the different activities between both inhibitors, are surrounded by residues Lys868, Cys1045, Asp1046, and Phe1047 (DFG motif).

We also used explicit-water MD calculations to analyze the movement of the systems and the effect of the solvent in the formation of the complexes. Throughout the MD simulations, the studied compounds were in the expected orientations. In both simulations, the NH of the oxindole group established a stable HB interaction with the backbone carbonyl group of Glu917, and the carbonyl group of the oxindole scaffold established a stable HB interaction with the backbone NH of Cys919 (Fig. 3). An intramolecular HB formed between the oxygen of the oxindole and the NH of the 3,5-dimethyl-1*H*-pyrrol-2-yl group was also stable during the MD simulations. The 3,5-dimethyl-1*H*-pyrrol-2-yl group did not form HBs with the residues at the entrance of the VEGFR-2 binding site and was almost planar with respect to the oxindole scaffold, while the {[2-(diethylamino)ethyl]amino}carbonyl group was exposed to the solvent, and had a high mobility for both systems.

We estimated the binding-free energy (ΔG_{calc_bind}) of each ligand using Prime molecular mechanics-generalized Born surface area (MM-GBSA) method [27,35]. The calculations were performed on each complex system using twenty snapshots from the MD simulations. The following equation (1) was used:

$$\Delta G_{calc\_bind} = \Delta E_{MM} + \Delta G_{solv} - T\Delta S \quad (1)$$

In (1) ΔE_{MM} is the change of the gas phase MM energy upon binding, and includes $\Delta E_{internal}$ (bond, angle, and dihedral energies), ΔE_{elect} (electrostatic), and ΔE_{vdw} (van der Waals) energies. ΔG_{solv} is the change of the solvation free energy upon binding, and includes the electrostatic solvation free energy ΔG_{solvGB} (polar contribution calculated using generalized Born model), and the non-electrostatic solvation component ΔG_{solvSA} (nonpolar contribution estimated by solvent accessible surface area). Finally, $T\Delta S$ is the change of the conformational entropy upon binding; this term was calculated using normal-mode analysis RRHO contained in MacroModel module [30]. The averaged energy values obtained from MM-GBSA calculations are reported in Table 2. The experimental binding-free energy values (ΔG_{exp_bind}) derived from K_i values are −10.964 and −10.491 kcal/mol for the complexes of sunitinib® and 5-methoxy-sunitinib **5** respectively. The difference between these values is 0.473 kcal/mol only. This is a small difference, and small differences are hard to calculate precisely using computational methods. The calculated binding-free energy value (ΔG_{calc_bind}) showed that both complexes have similar binding affinities (the difference in the ΔG_{calc_bind} value between both inhibitors was 0.346 kcal/mol).

According to the energy components of the binding free energies (Table 2), the major favorable contributors to ligand binding are VDW and electrostatic terms, whereas polar solvation (ΔG_{solvGB}) and entropy terms oppose binding. Nonpolar solvation terms (ΔG_{solvSA}) contribute slightly unfavorably for the complex. If we examine the contributions to each binding energy, the term ΔE_{elect} suggests a difference in the binding affinity. The better binding of sunitinib® gains over 4.697 kcal/mol of ΔE_{elect} value compared with 5-methoxy-sunitinib **5**, which influences the more favorable binding-free energy value for sunitinib®. However, the term ΔE_{vdw} compensates for this difference in the binding affinity, since 5-methoxy-sunitinib **5** has a more favorable value of ΔE_{vdw} (4.024 kcal/mol) compared with sunitinib®.

This suggests that sunitinib® establishes better electrostatic interactions and 5-methoxy-sunitinib **5** established better VDW interactions with VEGFR-2 residues. We analyzed the MD trajectories to explain this paradigm. We focused on the residues located in the surroundings of the groups at position 5 of oxindole scaffold (F or OCH_3), which are responsible of the different activities between both inhibitors. We identified that several water molecules occupy a position between the fluoro-group of sunitinib® and the side chain of Asp1046 (DFG motif) during the MD simulation of the complex VEGFR-2/sunitinib® (Fig. 3A). The presence of these water molecules suggests that a water-mediated HB bridge connecting the fluorine of sunitinib® with the oxygens of the carboxylate of Asp1046 can be formed. The HB acceptor capability of halogens has been recognized in recent literature; however, current molecular mechanics (MM) simulations, which rely primarily upon empirical force fields that in general do not explicitly account for electronic polarization, appear to be not appropriate for describing the involvement of halogens in HBs [36,37]. In this sense, the presence of halogen-mediated HBs cannot be confirmed using MM methods. On the other hand, we identified that several water

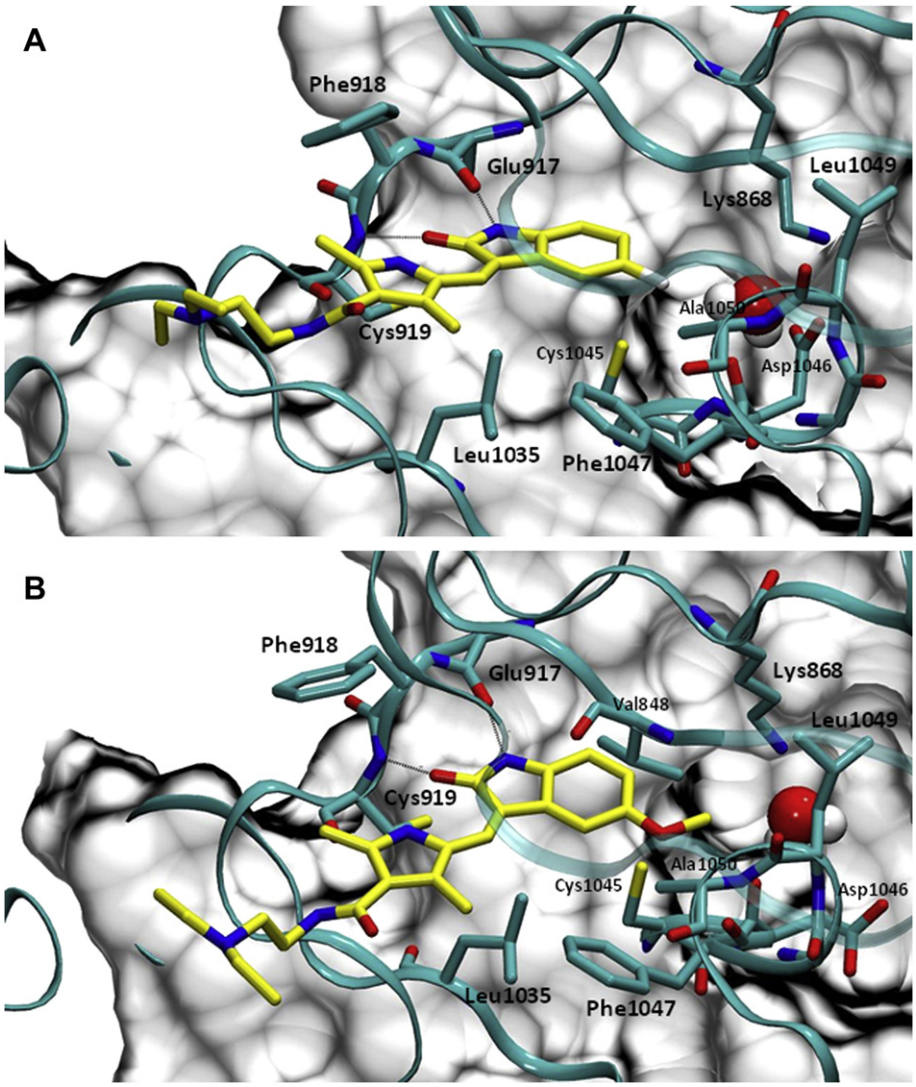

Fig. 3. Proposed docked structures of VEGFR-2/inhibitor complexes after rigid docking and MD simulation: (A) VEGFR-2/sunitinib®, (B) VEGFR-2/compound **5**; water molecules in the surroundings of the groups at position 5 of oxindole scaffold (F or OCH_3) are represented with a *space-filling representation*.

molecules occupy a position between the NH_3^+ side-chain group of Lys868 and the side-chain of Asp1046 during the MD simulation of the complex VEGFR-2/compound **5** (Fig. 3B). These water molecules were located close to the methyl group of the OCH_3 at position 5 of oxindole scaffold of 5-methoxy-sunitinib **5**, which could lead to unfavorable interactions. This analysis suggests that the fluoro-group has more favorable electrostatic interactions with the polar groups of the residues of VEGFR-2, which can explain the more favorable value of the ΔE_{elect} value of sunitinib®. During the MD dynamics, the methoxy-group at position 5 of oxindole scaffold of 5-methoxy-sunitinib **5** established favorable VDW interactions with the hydrophobic residues Ala1050, Val848, and Cys1045 (Fig. 3B). The methoxy-group is bulkier than the fluoro-group, making its VDW interactions with the above-mentioned residues much more compact. This fact explains the more favorable value of the ΔE_{vdw} value of 5-methoxy-sunitinib **5**.

4.4. Radiochemistry

The radiosynthesis of 5-[^{11}C]methoxy-sunitinib [^{11}C]-**5** was performed in a remotely controlled TracerLab$_{FxC}$ gas phase synthesizer (GE) via O-methylation reaction of the corresponding desmethyl precursor **4** with [^{11}C]CH_3I as the methylation reagent (Scheme 2). The synthesis started from [^{11}C]CH_4 produced in the cyclotron by irradiation of nitrogen containing 10% hydrogen gas in an aluminum target as described by Buckley et al. [38]. The [^{11}C]CH_4

Table 2
Calculated binding free energies for VEGFR2–ligand complexes using MM-GBSA for the snapshots of MD simulations.

Complex	$\Delta E_{internal}$ (kcal/mol)	ΔE_{elect} (kcal/mol)	ΔE_{vdw} (kcal/mol)	ΔG_{solvGB} (kcal/mol)	ΔG_{solvSA} (kcal/mol)	$T\Delta S$ (kcal/mol)	ΔG_{bind} (kcal/mol)
Sunitinib–VEGFR2	1.333 ± 1.153	−20.845 ± 1.435	−48.620 ± 1.888	18.441 ± 3.199	2.636 ± 1.316	−16.781 ± 0.910	−26.956 ± 3.107
5–VEGFR2	1.523 ± 0.884	−16.147 ± 2.656	−52.644 ± 2.211	19.859 ± 2.315	2.314 ± 0.806	−17.793 ± 0.897	−27.302 ± 2.437
Difference (absolute values)	0.190	4.697	4.024	1.418	0.322	1.012	0.346

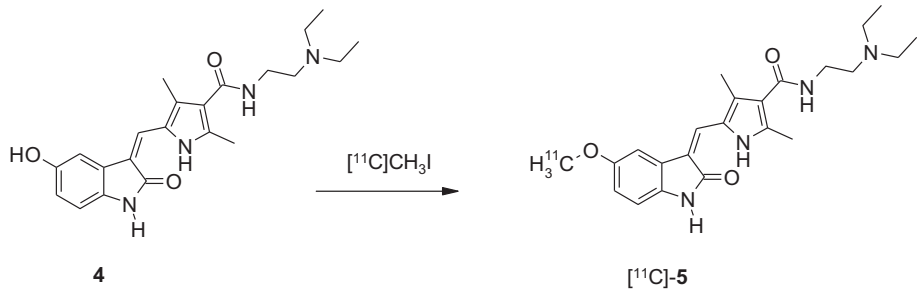

4 [11C]-5

Scheme 2. Radiosynthesis of 5-[^{11}C]methoxy-sunitinib ([^{11}C]-**5**).

was trapped on a carbosphere® trap at −140 °C and after release converted to [^{11}C]CH_3I by a gas phase iodination at 720 °C [39]. Then, the desmethyl precursor **4**, dissolved in DMF, reacted with [^{11}C]CH_3I in the presence of aqueous NaOH at 80 °C for 3 min: The reaction mixture was analyzed by radio-HPLC for characterization. From the chromatogram analysis it was evident that aside from the desired radiotracer [^{11}C]-**5** and unreacted [^{11}C]CH_3I a third ^{11}C-methylated product was formed in radiochemical yields ranging between 17 and 41%. Taking into consideration the chemical structure of sunitinib® that comprises a pyrrole and an oxindole moiety both bearing acidic hydrogens, an N-methylation reaction was expected to occur. A set of experiments were carried out in which different amounts of base were used in order to successfully decrease the formation of the side-product. Finally, reaction of 1.5 equiv of NaOH with 1.0 equiv of labeling precursor increased the formation of the desired radiotracer [^{11}C]-**5** in the labeling mixture to a 40% yield .The labeled raw material was purified by semi-preparative HPLC using as eluent a mixture of acetonitrile/0.02 M Na_2HPO_4 = 65/35 (v/v) to accomplish an efficient separation of [^{11}C]-**5** from the labeling precursor and the radiolabeled side-product. Due to the alkaline analytical conditions of the mobile phase a semi-preparative PRP-1 column was used. The fraction of [^{11}C]-**5** eluted at R_t = 8–9 min was collected and separated by solid phase extraction. After reconstitution with E153 solution the radiotracer was suitable for further animal experiments. Under these conditions [^{11}C]-**5** was obtained in 17 ± 3% decay-corrected radiochemical yield at a specific activity of 162–205 GBq/μmol at the end of synthesis. The identity of the radiotracer was confirmed by co-injection with the non-radioactive reference compound **5** in analytical HPLC system. The radiochemical purity of the final product was higher than 96% and the obtained specific activity equals in average a total amount of 0.3 μg/mL of non-radioactive **5** in the final product solution.

4.5. In vitro stability studies

The metabolism of 5-[^{11}C]methoxy-sunitinib [^{11}C]-**5** was investigated *in vivo* by analysis of arterial blood plasma samples of rats taken at different time points after injection of the radiotracer. The plasma was separated by blood centrifugation, treated with methanol to precipitate plasmatic proteins and analyzed by radio-HPLC. The amount of the intact radiotracer [^{11}C]-**5**, in blood samples, expressed as % of total radioactivity, over post injection time for two separate experiments is depicted in Fig. 4. As can be observed in Fig. 4, [^{11}C]-**5** exhibits relatively high stability in blood up to 60 min since a major radiochemical species with retention time similar to that of the injected compound (72% and 73%, respectively) could be detected in blood plasma. On the other hand analysis of plasma samples taken 10 min after injection demonstrated that 18–28% of the injected compound has been already metabolized and no relevant change was found for the following 50 min. In HPLC analyses of plasma samples taken 1 h after injection, the radiotracer [^{11}C]-**5** was eluted with retention time about 14 min and three other less lipophilic radioactive metabolites were detected with R_t = 4 min, 12.5 min and 13.5 min respectively (Fig. 5). However an amount of more than 70% of the intact radiotracer detectable 60 min post injection suggests a relatively high *in vivo* metabolic stability of [^{11}C]-**5**.

5. Conclusion

The search for radiolabeled probes toward VEGFR expression and for *in vivo* monitoring processes involved in tumor proliferation and angiogenesis, suggested us the development of a radiolabeled derivative of sunitinib®. We focused on radiolabeling with the positron emitting isotope carbon-11, therefore a 5-methoxy-substituted sunitinib® derivative was synthesized as non-radioactive reference and a 5-hydroxyl-substituted sunitinib® was developed as labeling precursor. The novel 5-methoxy-sunitinib **5** was identified as a VEGFR-2 inhibitor with a K_d value of 20 nM. The ability of **5** to inhibit cell proliferation was assessed by the colorimetric MTT assay in two VEGFR expressing cell lines and revealed that the compound is able to cross the cell membrane and inhibit the cell propagation. However in comparison to sunitinib® it turned out that the potency of **5** to act as inhibitor is lower and is cell line-dependent.

Docking simulations were performed to describe the binding of the methoxy-substituted compound **5** to VEGFR-2 and to compare it with sunitinib®. Both inhibitors are orientated in a similar manner; groups at position 5 of the oxindole scaffold could interact with residues near the DFG motif of VEGFR-2. The presence of the fluoro-substituent at position 5 of the oxindole scaffold in sunitinib® favors electrostatic interactions with polar VEGFR-2 residues. When the fluorine is substituted by a methoxy-group, electrostatic interactions become unfavorable, but more compact VDW interactions are established with hydrophobic VEGFR-2 residues. As a result, both inhibitors are predicted with similar

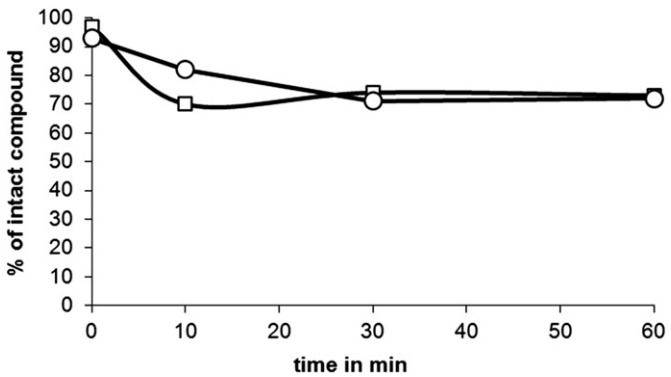

Fig. 4. Metabolic stability of 5-[^{11}C]methoxy-sunitinib [^{11}C]-**5** *in vivo* expressed as % of total radioactivity (n = 2).

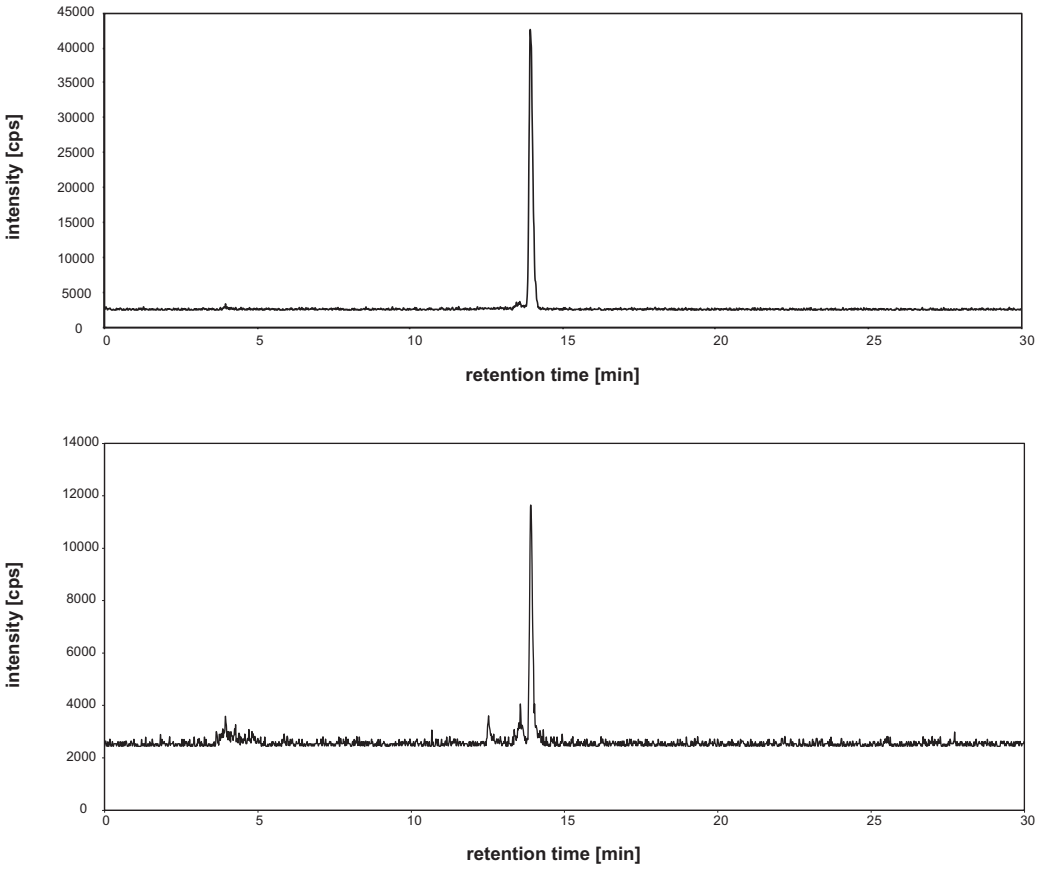

Fig. 5. Analytical radio HPLC of [^{11}C]-**5** from plasma; top: 3 min past injection; bottom: 60 min past injection.

binding-free energy values, which is in agreement with the *in vitro* binding assay.

The ^{11}C-radiolabeled analog [^{11}C]-**5** was obtained in 17 ± 3% decay-corrected radiochemical yield at a specific activity of 162–205 GBq/μmol at the end of synthesis, radiochemical purity of [^{11}C]-**5** exceeded 96%. *In vivo* stability studies of the radiotracer in rat blood revealed that the compound is satisfactory stable, hence 60 min after injection more than 70% of the original compound could be detected.

In summary, these preliminary pharmacological data suggest that 5-methoxy-sunitinib **5** is an inhibitor of VEGFR-2 albeit showing a slightly lower potency as the lead compound and the corresponding radiotracer [^{11}C]-**5** has provided evidence of metabolic *in vivo* stability. Thus, these results indicate that this compound can be a promising imaging agent of VEGFR-2 tyrosine kinase expressing cells and further investigations to evaluate its potential as radiotracer for angiogenesis and carcinogenesis are worthwhile.

6. Experimental

6.1. Chemistry

All commercial reagents and solvents were used without further purification unless otherwise specified. Melting points were determined with an apparatus Galen™III (Cambridge Instruments) and are uncorrected. Nuclear magnetic resonance spectra were recorded on a Unity 400 MHz spectrometer (Varian). ^{1}H NMR chemical shifts were given in ppm and were referenced with the residual solvent resonances relative to tetramethylsilane (TMS). Mass spectra were obtained with a Quattro/LC mass spectrometer (Micromass) by electrospray ionization. Flash chromatography was conducted using MERCK silica gel (mesh size 230–400 ASTM). Thin-layer chromatography (TLC) was performed on MERCK silica gel F-254 aluminum plates with visualization under UV (254 nm).

6.1.1. 5-Hydroxy-2-oxindole ***1***

Compound **1** was prepared as described in Itoh et al. [22]: 799 mg (6.0 mmol) of oxindole were dissolved at room temperature in 40 mL of water–free dichloromethane 3.1 g (7.2 mmol) of phenyliodine(III)-bis(trifluoroacetate) PIFA was added in portions, followed by 4.6 mL of trifluoroacetic acid. The mixture was stirred at RT overnight and the dichloromethane was evaporated. 60 mL of 5% sodium bicarbonate solution and 50 mL of ethyl acetate were added to the residue and the organic layer was separated by a separatory funnel. The aqueous layer was extracted with ethyl acetate (5 × 50 mL) the combined organic layer was dried with Na_2SO_4, filtered and evaporated under reduced pressure. The crude product was purified by column chromatography (silica gel, dichloromethane/methanol = 9:1 (v/v)) and afforded 627 mg (70%) of **1** as light brown crystals. Mp: 266–268 °C (lit: 260–263 °C), ^{1}H NMR (δ, ppm, DMSO-d_6): 3.36 (s, 2H, H-3); 6.55 (d, 1H, ^2J = 8.6 Hz, H-6); 6.60 (d, 1H, ^2J = 8.7 Hz, H-7); 6.66 (s, 1-H, H-4); 8.93 (s, 1H, OH); 10.47 (s, 1H, NH); ESI-MS (ES-): m/z = 148 [M − H].

6.1.2. 5-Methoxy-2-oxindole ***2***

The compound was prepared as described at Laksmaiah et al. [23]: 179 mg (1.2 mmol) of **1** was dissolved in 1.3 mL of 1.0 M KOH solution and cooled to 0 °C. Dimethyl sulfate (124 μL, 1.3 mmol) was added and stirring was continued for 2 h, after dilution with 15 mL water the mixture was extracted with ethyl acetate (3 × 15 mL). The combined organic layer was dried with Na_2SO_4, filtered and evaporated under reduced pressure. After column chromatographic purification (silica

gel, dichloromethane/methanol = 95:5 v/v) 69 mg (35%) **2** was obtained as crystals. Mp: 144–148 °C (lit: 148–151 °C), ESI-MS (ES+): $m/z = 164$ [M + H].

6.1.3. 5-[5-Hydroxy-2-oxo-1,2-dihydro-indol-(3-Z)-ylidenemethyl]-2,4-dimethyl-1H-pyrrole-3-carboxylic acid (2-diethylamino-ethyl)-amide ***4***

In a 25 mL flask 210 mg (1.4 mmol) **1** and 445 mg (1.68 mmol) *N*-[2-(diethylamino)ethyl]-2,4-dimethyl-5-formyl-1*H*-pyrrole-3-carboxamide **3** [24] were dissolved in 10 mL of ethyl alcohol and five drops of piperidine were added. After 4 h of refluxing **4** was formed as a red precipitate that after cooling was filtered of and washed with small amounts of ethyl alcohol and petrol ether. The collected red crystals were dried under vacuum and yielded 340 mg (61%) of **4**. Mp: 262–266 °C, ^{1}H NMR (δ, ppm, DMSO-d_6): 0.92 (t, 6H, 2 × CH_3), 2.34 (s, 3H, $CH_{3/pyrrole}$), 2.38 (s, 3H, $CH_{3/pyrrole}$), 2.46 (m, 6H, 3 × CH_2), 3.21 (q, 2H, CH_2), 6.51 (m, 1H, CH), 6.60 (d, 1H, CH), 7.12 (d, 1H, CH), 7.34 (t, 1H, CONH), 7.44 (s, 1H, CH_{vinyl}), 8,89 (s, 1H, OH), 10.55 (s, 1H, $NH_{oxindole}$), 13.67 (s, 1H, $NH_{pyrrole}$), ^{13}C NMR (δ, ppm, DMSO-d_6): 10.45 (CH_3), 11.83 (CH_3), 13.52 (CH_3), 36.95 (CH_2), 46.42 (CH_2), 51.59 (CH_2), 105.89, 109.73, 113.26, 115.87, 120.22, 123.01, 125.05, 126.44, 128.58, 131.07, 135.34, 152.39 (12 × C═C), 164.57 (C═O), 169.33 (C═O), ESI-MS (ES+): $m/z = 397.43$ (M + H).

6.1.4. 5-[5-Methoxy-2-oxo-1,2-dihydro-indol-(3-Z)-ylidenemethyl]-2,4-dimethyl-1H-pyrrole-3-carboxylic acid (2-diethylamino-ethyl)-amide ***5***

In a 10 mL flask 94 mg (0.58 mmol) **2** and 171 mg (0.64 mmol) **3** [24] were dissolved in 3.0 mL of ethyl alcohol, four drops of piperidine were added and the mixture was refluxed for 4 h. The solution was allowed to cool and stored in a refrigerator overnight. The orange crystals that have precipitated were filtered and washed with small amounts of ethyl alcohol and petrol ether and yielded after drying under vacuum 107 mg (45%) of **5**. Mp: 220–222 °C, ^{1}H NMR (δ, ppm, DMSO-d_6): 0.99 (t, 6H, 2 × CH_3), 2.45 (s, 3H, $CH_{3/pyrrole}$), 2.46 (s, 3H, $CH_{3/pyrrole}$), 2.52 (m, 6H, 3 × CH_2), 3.29 (q, 2H, CH_2), 3.79 (s, 3H, CH_3O), 6.71 (m, 1H, CH), 6.78 (d, 1H, CH), 7.42 (t, 1H, CONH), 7.50 (d, 1H, CH), 7.68 (s, 1H, CH_{vinyl}), 10.72 (s, 1H, $NH_{oxindole}$), 13.76 (s, 1H, $NH_{pyrrole}$), ^{13}C NMR (δ, ppm, DMSO-d_6): 10.63 (CH_3), 11.84 (CH_3), 13.23 (CH_3), 36.90 (CH_2), 46.43 (CH_2), 51.56 (CH_2), 55.56 (OCH_3), 104.44, 109.80, 112.54, 115.60, 120.27, 13.64, 125.62, 126.40, 129.00, 132.19, 135.65, 154.81 (12 × C═C), 164.52 (C═O), 169.42 (C═O), ESI-MS (ES+): $m/z = 411.42$ (M + H).

6.2. Biology

6.2.1. Inhibition of cell proliferation by MTT assay

6.2.1.1. Cell lines. Cellular studies were carried out in human aortic endothelial cells (HAECs) and in a VEGFR-expressing cell line (HT29) from a human colorectal adenocarcinoma. Primary endothelial cells were cultured in Cell Growth Medium MV2 (Promocell) supplemented with 1% penicillin/streptomycin and routinely passaged and only cells between passage 4 and 7 were used in the assays. Tumor cells were grown in McCoy's 5A medium (Gibco) supplemented with 10% fetal bovine serum and 1% penicillin/streptomycin under a humidified 5% CO_2 atmosphere at 37 °C. Cells were subcultured every 2 or 3 days.

6.2.1.2. MTT assay. The cells were seeded in a 96-well plate at a density of 7500 cells per 200 μL per well and incubated for 24 h for attachment to the wells. The day after seeding, exponentially growing cells were incubated with various concentrations of the compounds (**5** and sunitinib®) (ranging from 1 nM to 100 μM in 4 replicates) for 72 h. Controls consisted of wells without any compound. The medium was removed and the cells were incubated for 3 h in the presence of 0.5 mg mL^{-1} MTT (3-[4,5-dimethylthiazol-2-yl]-2,5-diphenyltetrazolium bromide, Sigma) in PBS (Gibco, Invitrogen, UK) at 37 °C. The MTT solution was removed and 200 μL per well of DMSO was added. After thorough mixing, absorbance of the wells was read in an ELISA reader at test and reference wavelengths of 570 nm. The mean of the optical density of different replicates of the same sample and the percentage of each value was calculated (mean of the OD of various replicates/OD of the control). The percentage of the optical density against compound concentration was plotted on a semilog chart and the IC_{50} from the dose–response curve was determined. Three cell proliferation assays were performed for each of the three compounds.

6.2.2. Metabolite analysis

Male Wistar-Unilever rats ($n = 2$; body weight 150 ± 12 g) were anesthetized with desflurane (9–10% v/v, 30% oxygen/air). The threshold value for breathing frequency was 65 breaths/min. Animals were put in supine position and placed on a heating pad to maintain body temperature. The spontaneously breathing rats were heparinized with 100 units/kg heparin (Heparin-Natrium 25.000-ratiopharm®, ratiopharm GmbH, Germany) by subcutaneous injection to prevent blood clotting on intravascular catheters. After local anesthesia with lignocain (1%; Xylocitin® loc, mibe, Jena, Germany) into the right groin, a catheter (0.8 mm Umbilical Vessel Catheter, Tyco Healthcare, Tullamore, Ireland) was introduced into the right femoral artery for arterial blood sampling. A second needle catheter (35 G) was placed into a tail vein and was used for [^{11}C]-**5** radiotracer injection (39 MBq in 0.5 mL of E153/10% ethanol, infusion 1 mL/min). Arterial blood samples were taken 1.5, 10, 30 and 60 min after injection. Arterial plasma was separated by centrifugation (11.000 g × 3 min) followed by precipitation of the proteins with methanol (2 volumes to 1 volume plasma) followed by 5 min storage at −60 °C. The clear supernatant separated by centrifugation was used for analysis. The radio-HPLC system (Agilent 1100 series) applied for metabolite analysis was equipped with UV detection (254 nm) and an external radiochemical detector (RAMONA, Raytest GmbH, Germany). Analysis was performed on a Zorbax C18 300SB (250 × 9.4 mm; 4 μm) column with an eluent system C (water + 0.1% TFA) and D (acetonitrile + 0.1% TFA) in the following gradient: 5 min 95% C, 10 min to 95% D, 5 min at 95% D and 5 min to 95%C at a flow rate of 3 mL/min.

6.3. Radiochemistry

[^{11}C]CH_4 was produced by the ^{14}N(p,α)^{11}C reaction in a CYCLONE 18/9 cyclotron (IBA) by irradiation of nitrogen gas containing 10% hydrogen gas in an aluminum target. Radiosynthesis and semi-preparative purification was performed in an automated nucleophilic synthesizer $TracerLab_{FxC}$ (GE) that was modified in terms of direct trapping of [^{11}C]CH_4. Semi-preparative HPLC purifications were carried out with a PRP1 column (250 × 10 mm, 5 μm, Hamilton) using an isocratic eluent of acetonitrile/0.02 M Na_2HPO_4 = 65/35 (v/v) by an S1122 HPLC-pump (Sykam) with a flow rate of 4 mL/min. The product was monitored by a K-2001 filter photometer (Knauer) at 254 nm and by a gamma-detector integrated in the synthesizer module. Analytical HPLC investigation was performed with a C18 column (250 × 4 mm, 5 μm, Nucleodur Isis, Macherey–Nagel) using a gradient eluent of acetonitrile (A) and water containing 0.1% TFA (B) by an L2500 pump (MERCK, Hitachi) with a flow rate of 1.0 mL/min. The gradient was as follows: 0.0 min–7.0 min (10% A–95% A); 7.0 min–9.0 min (95% A–100% A); 9.0 min–10 min (100% A–10% A). The products were monitored by an UV detector L4500 (Merck, Hitachi) at 276 nm and by a gamma scintillation detector GABI (Raytest).

*6.3.1. 5-[5-[^{11}C]methoxy-2-oxo-1,2-dihydro-indol-(3-Z)-ylidenemethyl]-2,4-dimethyl-1H-pyrrole-3-carboxylic acid (2-diethylamino-ethyl)-amide [^{11}C]-**5***

Labeling precursor **4** (1.0 mg, 2.5 μmol) dissolved in 250 μL DMF and 40 μL 0.1 M aqueous NaOH was placed in the reacting vessel of the synthesizer unit. [^{11}C]CH_3I was transferred in a stream of helium into the reaction vessel at a temperature of −20 °C. After completion of the transfer, the reaction vessel was sealed and heated at 80 °C for 3 min. The reactor was cooled to 40 °C, 1 mL of acetonitrile was added and the mixture was transferred onto a semi-preparative PRP 1 column. The product eluting between 8 and 9 min was separated and diluted with 30 mL of water and passed through an SPE-cartridge (Lichrolut, RP18, 500 mg). The product was eluted from the cartridge with 0.75 mL of ethanol and reconstituted with 6.5 mL of E153 solution. In a typical experiment 970 MBq of compound [^{11}C]-**5** could be obtained within 24 min after EOB starting from 13,500 MBq of [^{11}C]CH_4 (17% decay corrected radiochemical yield based upon [^{11}C]CH_4). The specific activity was determined to be 198 GBq/μmol at the end of synthesis.

Acknowledgments

The authors want to thank Lars Ruddigkeit, Department of Chemistry and Biochemistry at the University of Bern (Switzerland) for helpful discussions. The authors wish to thank S. Preusche for radioisotope production and A. Suhr and P. Wecke for expert technical assistance.

References

[1] J. Folkman, Tumor angiogenesis: therapeutic implications, N. Engl. J. Med. 285 (1971) 1182–1186.
[2] W.P. Leenders, B. Küsters, R.M. de Waal, Vessel co-option: how tumors obtain blood supply in the absence of sprouting angiogenesis, Endothelium 9 (2002) 83–87.
[3] N. Ferrera, Vascular endothelial growth factor: basis science and clinical progress, Endocr. Rev. 25 (2004) 581–611.
[4] M. Shibuya, L. Claesson-Welsh, Signal transduction by VEGF receptors in regulation of angiogenesis and lymphagogenesis, Exp. Cell. Res. 312 (2006) 549–560.
[5] J.W. Hicks, H.F. Van Brocklin, A.A. Wilsom, S. Houle, N. Vasdev, Radiolabeled small molecule protein kinase inhibitors for imaging with PET or SPECT, Molecules 15 (2010) 8260–8278.
[6] M.H. Michalski, X. Chen, Molecular imaging in cancer treatment, Eur. J. Nucl. Med. Mol. Imaging 38 (2011) 358–377.
[7] V. Tolmachev, S. Stone-Elander, A. Orlova, Radiolabelled receptor-tyrosine-kinase targeting drugs for patient stratification and monitoring of therapy response: prospects and pitfalls, Lancet Oncol. 11 (2010) 992–1000.
[8] R. Haubner, H.J. Wester, W.A. Weber, M. Schwaiger, Radiotracer-based strategies to image angiogenesis, Q. J. Nucl. Med. 47 (2003) 189–199.
[9] R. Haubner, H.J. Wester, Radiolabeled tracers for imaging tumor angiogenesis and evaluation of anti-angiogenic therapies, Curr. Pharm. Des. 10 (2004) 1439–1455.
[10] E. Samen, J.O. Thorell, L. Lu, T. Tegnebratt, L. Holmgren, S. Stone-Elander, Synthesis and preclinical evaluation of [^{11}C]PAO as PET imaging tracer for VEGFR-2, Eur. J. Nucl. Med. Mol. Imaging 36 (2009) 1283–1295.
[11] O. Ilovich, O. Jacobson, Y. Aviv, A. Litchi, R. Chisin, E. Mishani, Formation of fluorine-18 labeled diaryl ureas – labeled VEGFR-2/PDGFR dual inhibitors as molecular imaging agents for angiogénesis, Bioorg. Med. Chem. 16 (2008) 4242–4251.
[12] O. Ilovich, O. Aberg, B. Langsröm, E. Mishani, Rhodium-mediated [^{11}C] carbonylation: a library of N-phenyl-N′-{4-(4-quinolyloxy)-phenyl}-[^{11}C]-urea derivatives as potential PET angiogenic probes, J. Label. Compd. Radiopharm. 52 (2009) 151–157.
[13] A. Chiharu, O. Masanao, K. Katsushi, F. Masayuki, K. Koichi, Y. Tomoteru, Y. Joji, K. Kazunori, H. Akiko, F. Toshimitsu, Z. Ming-Rong, Efficient radiosynthesis of [^{11}C]sorafenib using [^{11}C]phosgene as a labeling agent, J. Label. Compd. Radiopharm. 54-S1 (2011) S96.
[14] A.J. Poot, B. Van der Wildt, M. Stigter-van Walsum, R.C. Schuit, M. Rongen, G.A.M.S. Van Dongen, A.D. Windhorst, Two approaches for the synthesis of [^{11}C]sorafenib, a tyrosine kinase inhibitor PET tracer to be used in cancer therapy, J. Label. Compd. Radiopharm. 54-S1 (2011) S85.
[15] D. Dischino, T. Tran, D. Donelly, S. Bonascorsi, P. Chow, R. Roache, D. Kukral, J. Kim, W. Hayes, J. Label. Compd. Radiopharm. 54-S1 (2011) S444.
[16] O. Ilovich, H. Billauer, S. Dotan, E. Mishani, Labeled 3-aryl-4-indolylmaleimide derivatives and their potential as angiogenic PET biomarkers, Bioorg. Med. Chem. 18 (2010) 612–620.
[17] J.Q. Wang, K.D. Miller, G.W. Sledge, Q.H. Zheng, Synthesis of [^{18}F]SU11248, a new potential PET tracer for imaging cancer tyrosine kinase, Bioorg. Med. Chem. Lett. 15 (2005) 4380–4384.
[18] T. Kniess, R. Bergmann, M. Kuchar, J. Steinbach, F. Wuest, Synthesis and radiopharmacological investigation of 3-[4′-[18F]fluorobenzylidene]-indolin-2-one as possible tyrosine kinase inhibitor, Bioorg. Med. Chem. 17 (2009) 7733–7742.
[19] C. Muñoz, F. Adasme, J.H. Alzate-Morales, A. Vergara-Jaque, T. Kniess, J. Caballero, Study of differences in the VEGFR-2 inhibitory activities between semaxanib and SU5205 using 3D-QSAR, docking, and molecular dynamics simulations, J. Mol. Graph. Model. 32 (2012) 39–48.
[20] M. Kuchar, M.C. Oliveira, L. Gano, I. Santos, T. Kniess, Radioiodinated sunitinib as a potential radiotracer for imaging angiogenesis–radiosynthesis and first radiopharmacological evaluation of 5-[^{125}I]iodo-sunitinib, Bioorg. Med. Chem. Lett. (2012). http://dx.doi.org/10.1016/j.bmcl.2012.02.068.
[21] E. Giovannini, P. Portmann, Sur quelques derives de l'oxindole et de l'isatine. II. Sur les amino-, hydroxy- et méthoxy-dérivés substitués en position 5 et 6, Helv. Chim. Acta 31 (1948) 1381–1391.
[22] N. Itoh, T. Sakamoto, E. Miyazawa, Y. Kikugawa, Introduction of a hydroxyl group at the para position and *N*-iodophenylation of N-arylamides using phenyliodine(III)bis(trifluoroacetate), J. Org. Chem. 67 (2002) 7424–7428.
[23] G. Lakshmaiah, T. Kawabata, M. Shang, K. Fuji, Total synthesis of (−)-horsfiline via asymmetric nitroolefination, J. Org. Chem. 64 (1999) 1699–1704.
[24] L. Sun, C. Liang, S. Shirazian, Y. Zhou, T. Miller, J. Cui, J.Y. Fukuda, J.Y. Chu, A. Nematalla, X. Wang, H. Chen, A. Sistla, T.C. Luu, F. Tang, J. Wei, C. Tang, Discovery of 5-[5-fluoro-2-oxo-1,2-dihydroindol-(3*Z*)-ylidenemethyl]-2,4-dimethyl-1*H*-pyrrole-3-carboxylic acid (2-diethylaminoethyl)amide, a novel tyrosine kinase inhibitor targeting vascular endothelial and platelet-derived growth factor receptor tyrosine kinase, J. Med. Chem. 46 (2003) 1116–1119.
[25] R.A. Friesner, J.L. Banks, R.B. Murphy, T.A. Halgren, J.J. Klicic, D.T. Mainz, M.P. Repasky, E.H. Knoll, M. Shelley, J.K. Perry, D.E. Shaw, P. Francis, P.S. Shenkin, Glide: a new approach for rapid, accurate docking and scoring. 1. Method and assessment of docking accuracy, J. Med. Chem. 47 (2004) 1739–1749.
[26] J.H. Alzate-Morales, A. Vergara-Jaque, J. Caballero, Computational study on the interaction of N1 substituted pyrazole derivatives with B-raf kinase: an unusual water wire hydrogen-bond network and novel interactions at the entrance of the active site, J. Chem. Inf. Model. 50 (2010) 1101–1112.
[27] Maestro, Version 9.0, Schrödinger, LLC, New York, NY, 2007.
[28] G.A. Kaminski, R.A. Friesner, J. Tirado-Rives, W.L. Jorgensen, Evaluation and reparametrization of the OPLS-AA force field for proteins via comparison with accurate quantum chemical calculations on peptides, J. Phys. Chem. B 105 (2001) 6474–6487.
[29] K.J. Bowers, E. Chow, H. Xu, R.O. Dror, M.P. Eastwood, B.A. Gregersen, J.L. Klepeis, I. Kolossvary, M.A. Moraes, F.D. Sacerdoti, J.K. Salmon, Y. Shan, D.E. Shaw, in: Proceedings of the 2006 ACM/IEEE Conference on Supercomputing, ACM, Tampa, Florida, 2006, p. 84.
[30] MacroModel, Version 9.5, Schrödinger, LLC, New York, NY, 2007.
[31] W. Humphrey, A. Dalke, K. Schulten, VMD: visual molecular dynamics, J. Mol. Graph. 14 (1996) 33–38.
[32] M.A. Fabian, W.H. Biggs, D.K. Treiber, C.E. Atteridge, M.D. Azimioara, M.G. Benedetti, T.A. Carter, P. Cireci, P.T. Edeen, M. Floyd, J.M. Ford, M. Galvin, J.L. Gerlach, R.M. Grotzfeld, S. Herrgard, D.E. Insko, M.A. Insko, A.G. Lai, J.M. Lelias, S.A. Metha, Z.V. Milanov, A.M. Velasco, L.M. Wodicka, H.K. Patel, P.P. Zarrinkar, D.J. Lockhart, A small molecule-kinase interaction map for clinical kinase inhibitors, Nat. Biotechnol. 23 (2005) 329–336.
[33] D.B. Mendel, D.A. Laird, X. Xin, S.G. Louie, J.G. Christensen, G. Li, R.E. Schreck, T.J. Abrams, T.J. Ngai, L.B. Lee, L.J. Murray, J. Carver, E. Chan, K.G. Moss, J.Ö. Haznedar, J. Sukbuntherng, R.A. Blake, L. Sun, C. Tang, T. Miller, S. Shirazian, G. McMahon, J.M. Cherrington, In vivo antitumor activity of SU11248, a novel tyrosine kinase inhibitor targeting vascular endothelial growth factor and platelet-derived growth factor receptors: determination of a pharmacokinetic/pharmacodynamics relationship, Clin. Cancer Res. 9 (2003) 327–337.
[34] K.S. Gajiwala, J.C. Wu, J. Christensen, G.D. Deshmukh, W. Diehl, J.P. DiNitto, J.M. English, M.J. Greig, Y.A. He, S.L. Jacques, E.A. Lunney, M. McTigue, D. Molina, T. Quenzer, P.A. Wells, X. Yu, Y. Zhang, A. Zou, M.R. Emmett, A.G. Marshall, H.-M. Zhang, G.D. Demetri, KIT kinase mutants show unique mechanisms of drug resistance to imatinib and sunitinib in gastrointestinal stromal tumor patients, Proc. Natl. Acad. Sci. U.S.A. 106 (2009) 1542–1547.
[35] P.A. Kollman, I. Massova, C. Reyes, B. Kuhn, S. Huo, L. Chong, M. Lee, T. Lee, Y. Duan, W. Wang, O. Donini, P. Cieplak, J. Srinivasan, D.A. Case, T.E. Cheatham 3rd, Calculating structures and free energies of complex molecules: combining molecular mechanics and continuum models, Acc. Chem. Res. 33 (2000) 889–997.
[36] P. Zhou, J. Lv, J. Zou, F. Tian, Z. Shang, Halogen–water–hydrogen bridges in biomolecules, J. Struct. Biol. 169 (2010) 172–182.
[37] Y. Lu, Y. Wang, Z. Xu, X. Yan, X. Luo, H. Jiang, W. Zhu, C-X···H Contacts in biomolecular systems: how they contribute to protein-ligand binding affinity, J. Phys. Chem. B 113 (2009) 12615–12621.
[38] K.R. Buckley, J. Huser, S. Jivan, K.S. Chun, T.J. Ruth, ^{11}C-methane production in small volume, high pressure gas targets, Radiochem. Acta 88 (2000) 201–205.
[39] P. Larsen, J. Ulin, K. Dahlstrom, A new method for production of ^{11}C-labelled methyl iodide from ^{11}C-methane, J. Label. Compd. Radiopharm. 37 (1995) 73–75.